Endothelial Nox1 oxidase assembly in human pulmonary arterial hypertension; driver of Gremlin1-mediated proliferation

Imad Al Ghouleh[1,4,*], **Sanghamitra Sahoo**[1,3,*], **Daniel N. Meijles**[1,3], **Jefferson H. Amaral**[1], **Daniel S. de Jesus**[1,3], **John Sembrat**[1], **Mauricio Rojas**[1,4], **Dmitry A. Goncharov**[1], **Elena A. Goncharova**[1,4], and **Patrick J. Pagano**[1,3]

[1]Heart, Lung, and Blood Vascular Medicine Institute, University of Pittsburgh School of Medicine, Pittsburgh, PA, U.S.A

[2]Division of Cardiology, Department of Medicine, University of Pittsburgh School of Medicine, Pittsburgh, PA, U.S.A

[3]Department of Pharmacology and Chemical Biology, University of Pittsburgh School of Medicine, Pittsburgh, PA, U.S.A

[4]Division of Pulmonary, Allergy and Critical Care, University of Pittsburgh, Pittsburgh, PA, U.S.A

Abstract

Pulmonary arterial hypertension (PAH) is a rapidly degenerating and devastating disease of increased pulmonary vessel resistance leading to right heart failure. Palliative modalities remain limited despite recent endeavors to investigate the mechanisms underlying increased pulmonary vascular resistance (PVR), i.e. aberrant vascular remodeling and occlusion. However, little is known of the molecular mechanisms responsible for endothelial proliferation, a root cause of PAH-associated vascular remodeling. Lung tissue specimens from PAH and non-PAH patients and hypoxia-exposed human pulmonary artery endothelial cells (ECs) (HPAEC) were assessed for mRNA and protein expression. Reactive oxygen species (ROS) were measured using cytochrome c and Amplex Red assays. Findings demonstrate for the first time an up-regulation of NADPH oxidase 1 (Nox1) at the transcript and protein level in resistance vessels from PAH compared with non-PAH patients. This coincided with an increase in ROS production and expression of bone morphogenetic protein (BMP) antagonist Gremlin1 (Grem1). In HPAEC, hypoxia induced Nox1 subunit expression, assembly, and oxidase activity leading to elevation in sonic hedgehog (SHH) and Grem1 expression. Nox1 gene silencing abrogated this cascade. Moreover, loss of either Nox1, SHH or Grem1 attenuated hypoxia-induced EC proliferation. Together, these data support a Nox1-SHH-Grem1 signaling axis in pulmonary vascular endothelium that is likely to contribute to

pathophysiological endothelial proliferation and the progression of PAH. These findings also support targeting of Nox1 as a viable therapeutic option to combat PAH.

Introduction

Despite the availability of a number of FDA-approved drugs, pulmonary arterial hypertension (PAH) remains a deadly disease with a median survival of 2.8 years from diagnosis [1,2]. Current therapies focus on dilation of the pulmonary vasculature in an attempt to attenuate pulmonary vascular resistance (PVR) and reduce right ventricle (RV) pressure overload which ultimately leads to right heart maladaptive hypertrophy and failure [3,4], the major cause of death in PAH [2]. However, currently there are no effective drugs that reverse the extensive vascular remodeling responsible for subsequent elevation of PVR. Endothelial dysfunction and proliferation are at the root of vascular remodeling in PAH [4–8], being associated with increased plexiform lesion (PL) formation and vascular occlusion [3,5]. Insight into the pathways governing endothelial proliferation in PAH remains scarce and, to date, no effective strategies exist which target increased endothelial cell (EC) proliferation in PAH.

Reactive oxygen species (ROS) and more recently NADPH oxidase (Nox) enzymes, have been implicated in the pathogenesis of PAH [9,10]. Nonetheless, this literature is surprisingly sparse and the role of Nox proteins in pulmonary EC proliferation is not known. Indeed, despite evidence supporting a role for the NADPH oxidase 1 (Nox1) isoform in systemic vascular proliferation and remodeling [11], little is known about the function for Nox1 in the pulmonary endothelium and PAH.

An *in silico* interactome suggested a potential link between Nox and the endogenous bone morphogenetic protein (BMP) antagonist Gremlin1 (Grem1) [12–15]. Grem1 is a 28-kDa member of the Differential screening-selected gene Aberrative in Neuroblastoma (DAN) family of glycoproteins [12] and functions as an antagonist of BMP2 and BMP4 signaling [12,13,15,16]. BMP4 signaling is associated with the maintenance of endothelial homeostasis, repair, and abated proliferation [14,17,18]. Thus, we postulated that EC Nox up-regulates Grem1 and leads to hyperproliferation in PAH. Indeed, the mechanisms by which Grem1 expression and secretion are regulated by Nox and ROS in PAH are entirely unknown.

The current study addresses a gap in knowledge of the mechanisms underlying endothelial proliferation in PAH. We report for the first time that Grem1 relaysNox1-mediated EC proliferation in an *in vitro* model of PAH, and draw strong preclinical and translational links amongst ROS, Nox1, and Grem1. Our data also identify sonic hedgehog (SHH), a pro-angiogenic factor [19], as an intermediary between Nox1 and Grem1 in EC.

Materials and methods

Materials and reagents

Cytochrome *c*, superoxide dismutase (SOD), catalase, diphenylene iodonium (DPI) chloride, PMSF, and dihydroethidium (DHE) were purchased from Sigma–Aldrich (St. Louis, MO,

U.S.A.). Amplex Red and propidium iodide were purchased from Life Technologies (Grand Island, NY, U.S.A.). Protease and phosphatase inhibitor cocktail tablets were purchased from Roche Diagnostics GmbH (Mannheim, Germany). Reagents and primers for qPCR were purchased from Life Technologies. Antibodies for Grem1, Nox1, p47^{phox}, and β-actin were purchased from Santa Cruz Biotechnology, Inc. (Dallas, TX, U.S.A.), and Nox organizer 1 (NoxO1) antibody was purchased from Rockland Immunochemicals. Nox activator 1 (NoxA1), SHH and BrdU antibodies were purchased from Abcam, (Cambridge, MA, U.S.A.). Carboxyfluorescein succinimidyl ester (CFSE) CellTrace™ Cell Proliferation Kit was purchased from Life Technologies.

Human tissue samples

Human tissue sample collection and processing were approved by the Institutional Review Board of the University of Pittsburgh. Lung tissue samples from PAH and non-PAH controls were obtained from human subjects who had given written consents. Tissues were collected either from recipient lungs during transplant surgery or during warm autopsy organ collection. Samples were de-identified with researchers performing the biochemical assays blinded to patient information. Samples were homogenized in ice-cold HBSS containing protease inhibitor cocktail tablets supplemented with PMSF using mortar and pestle and centrifuged at 1000×g to prepare homogenates from tissue samples. Protein concentrations were measured and samples were either processed for ROS measurement or Western blot analysis for protein expression. Demographic data of the non-PAH and PAH patient samples are provided in Table 1.

Sugen 5416/hypoxia rat model

All animal experiments were approved by the University of Pittsburgh Animal Care and Use Committee. To induce PAH, the SU5416 (Sugen)/hypoxia model was employed as previously described [20–22] with modifications. Female rats (7–10 per group; 250–275 g; Charles River Laboratories, Cambridge, MA) were injected with a single subcutaneous bolus of SU5416 (100 mg/kg, Sigma, St. Louis, MO) and subsequently subjected to hypoxia (10% O_2) for 3 weeks, followed by 1 week of normoxia (21% O_2). For ROS measurements, tissues were processed as detailed for human samples above.

Cell culture and treatment

Human pulmonary artery ECs (HPAEC; Lonza, Walkersville, MD, U.S.A.) were grown in EBM-2 medium containing EGM-2 bullet kit components (Lonza, Walkersville, MD, U.S.A.). Cells were seeded the day before experimentation and synchronized in serum-reduced medium (0.2% FBS) for 16 h prior to further experimentation. Cells between passages 3 and 6 were used in all the experiments. Hypoxic treatment *in vitro* was used to most closely resemble the *in vivo* disease as previously described [23–25]. Cells were incubated in either normoxia (21% oxygen) or hypoxia (1% oxygen) for 6, 12, 24, 36, or 48 h and subjected to either homogenization in ice-cold disruption buffer (HBSS containing 1.8 mM CaCl$_2$, 0.8 mM MgCl$_2$, and 0.1 mM protease inhibitor PMSF) or trypsinized for intact cell analysis. To gene silence Grem1, SHH, and Nox1, HPAEC were seeded at a density to achieve an overnight 75–80% confluence followed by transfection with Grem1, SHH, or

Nox1 siRNA or their scrambled control siRNA (Life Technologies) using the Lipofectamine 2000 transfection reagent (Life Technologies) according to the manufacturer's protocol as documented previously [26]. Gene silencing was confirmed using immunoblotting (detailed below) and knockdown expressed as a percent of siRNA-scrambled controls.

Quantitative real-time RT-PCR

Expression of mRNA was quantitated as previously described [26]. Briefly, total RNAs were extracted from human lung tissues and from HPAEC using the RNeasy Plus Mini Kit (Qiagen). Total RNA (1–2 μg) was reverse transcribed to cDNA using SuperscriptIII reverse transcriptase (Life Technologies) following the manufacturer's protocol. Taqman probe and Universal PCR Master Mix and Nox1, Grem1, p47^{phox}, NoxO1, NoxA1 or 18S primers (Life Technologies) were used for qPCR in a 7900HT Fast Real-Time PCR System (Life Technologies) according to the manufacturer's protocol for 40 cycles. Relative quantitation to corresponding control was obtained using the threshold cycle (Ct) method with 18S as the housekeeping gene and relative expression calculated as $2^{-\triangle\triangle Ct}$.

Western blot

Western blot experiments were performed as described previously [27,28]. Total protein (100 or 30 μg) from tissue homogenates or cell lysates, respectively, were added to Tris-glycine SDS sample buffer, boiled, resolved with SDS/PAGE, and transferred onto Trans-Blot nitrocellulose membranes (Bio–Rad). Membranes were blocked with the Odyssey Blocking Buffer (LI-COR Biosciences, Lincoln, NE) and incubated with rabbit anti-p47^{phox} (1:500 dilution, Santa Cruz Biotechnology), rabbit anti-Grem1 (1:250, Santa Cruz Biotechnology), goat anti-Nox1 (1:500, Santa Cruz Biotechnology), rabbit anti-NoxO1 (1:1000, Rockland Immunochemicals), rabbit anti-NoxA1 (1:1000, Abcam), mouse anti-SHH (1:1000, Abcam) or mouse anti-β-actin (1:2000, Santa Cruz Biotechnology). Membranes were probed with anti-rabbit, anti-mouse, or anti-goat secondary antibodies (1:10,000 dilution, LI-COR Biosciences). Digital imaging was obtained using the Odyssey Infrared Imaging system (LI-COR Biosciences). Optical density (OD) of protein-of-interest bands were quantitated and normalized to β-actin using ImageJ software (NIH, U.S.A.).

ROS measurement

Tissue homogenates or cell lysates were prepared for ROS measurement for assessment of $O_2^{\bullet-}$ production by the cytochrome c reduction assay or detection of 2-hydroxyethidium (2-OH-E$^+$) peaks by HPLC, and H_2O_2 production by the Amplex Red assay [26,27,29–31]. *Cytochrome c reduction assay* was conducted as described previously [26]. Briefly, HPAEC were washed twice with ice-cold PBS and 400 μl of ice-cold disruption buffer (8 mmol/l potassium sodium phosphate buffer, pH 7.0, 131 mmol/l NaCl, 340 mmol/l sucrose, 2 mmol/l NaN$_3$, 5 mmol/lMgCl$_2$, 1 mmol/l EGTA, 1 mmol/l EDTA, and protease inhibitor cocktail) was added. Cells were then scraped and subjected to five freeze/thaw cycles followed by five passages through a 30-gauge needle to lyse them. Lysates were centrifuged at 1000×g for 10 min at 4°C and the supernatant collected, and further centrifuged at 28000×g for 20 min at 4°C to collect the membrane fraction pellet, which was resuspended in 100 μl disruption buffer. Total homogenates (5 μg/well) or membrane fractions (5–10 μg/

well) were added to cytochrome c-containing oxidase assay buffer (65 mmol/l sodium phosphate buffer, pH 7.0, 1 mmol/l EGTA, 10 μmol/l FAD, 1 mmol/l MgCl$_2$, 2 mmol/l NaN$_3$, 0.2 mmol/l cytochrome c and 1000 U/ml catalase) and $O_2^{\bullet-}$ was measured as the initial rate of SOD (150 U/ml)-inhibitable cytochrome c reduction quantitated at 550 nm using the extinction coefficient 21.1 mmol^{-1}•l cm^{-1} on a Biotek Synergy 4 Hybrid Multi-Mode Microplate Reader. After a 5-min baseline measurement, NADPH (180 μmol/l) was added and $O_2^{\bullet-}$ production was calculated from the initial linear rate (first 10 min) of cytochrome c reduction. ***H_2O_2 production by Amplex Red assay*** was measured in tissue homogenates as described previously [27]. Briefly, frozen human lung samples were homogenized in HBSS-containing protease inhibitors cocktail (Roche Diagnostics GmbH, Mannheim, Germany), Phospho-Stop cocktail (Roche Diagnostics GmbH, Mannheim, Germany), and 0.1 mM PMSF. The homogenates were centrifuged at 1000×***g*** for 10 min at 4°C in order to sediment undisrupted tissue, and an appropriate amount of supernatant (equivalent to 10 μg of protein) was loaded into black 96-well plates in assay buffer (25 mM Hepes, pH 7.4 containing 0.12 M NaCl, 3 mM KCl, 1 mM MgCl$_2$, 0.1 mM Amplex Red, and 0.32 U/ml HRP) in the presence or absence of catalase 3000 U/ml, DPI 20 μM, or SOD 200 U/ml. The reaction was initiated by the addition of 36 μM NADPH. Fluorescence was measured using a Biotek Synergy 4 Hybrid Multi-Mode Microplate Reader with a 530/25-excitation and a 590/35-emission filter, for 30 min at 25°C. The catalase-inhibitable rate of H_2O_2 production was quantitated from an H_2O_2 standard curve. ***Intracellular $O_2^{\bullet-}$ detection by DHE-HPLC*** in intact HPAEC was measured as described previously [30]. Briefly, HPAEC were pre-incubated with DHE (10 μM) for 30 min prior to ice-cold PBS wash, collection, and lysis using 0.1% Triton X buffer. Cells were passed through a 30-gauge needle to ensure lysis, and centrifuged at 1000×***g*** for 5 min at 4°C to remove unbroken cells. Proteins were precipitated out using methanol and lysates were run on a HPLC system equipped with a fluorescence detector to monitor the specific 2-OH-E$^+$ $O_2^{\bullet-}$ peak, as published previously [30]. Results were normalized to protein concentrations and $O_2^{\bullet-}$ using a 2-OH-E$^+$ standard curve.

Cell proliferation assay

Proliferation of HPAEC was measured by the CFSE CellTrace™ Cell Proliferation Kit using FACS, by BrdU incorporation using ELISA method or by the CyQuant® assay. CFSE FACS assay was conducted as described previously [28]. Briefly, HPAEC seeded into six-well tissue culture dishes were transfected with Grem1 siRNA or scrambled, and serum deprived (0.2% FBS) for 24 h. After the requisite time, cells were incubated with 1.25 μM CFSE for 15 min. Cells were then washed with PBS and incubated under normoxic or hypoxic conditions for 24 h. Cells incubated for 24 h in the presence of complete growth medium were used as positive controls. CFSE fluorescence was evaluated by flow cytometry analysis using a BD LSRFortessa™ cell analyzer and data were analyzed using FlowJo (version 10). For BrdU incorporation, HPAEC transfected with Nox1 siRNA or scrambled were labeled with 10 μM BrdU (Sigma) and exposed to 21% or 1%O$_2$ for 24 h. Twenty nanograms of protein was loaded onto a 96-well plate in binding buffer and incubated overnight at 4°C. The amount of BrdU incorporation was measured by direct ELISA using anti-BrdU antibody (Abcam), and developed using ABTS substrate (Pierce Bio.). The reaction product was quantitated by measuring the absorbance at 405 nm with a reference wavelength of 650

nm. Data are presented as a fold change from normoxic controls. For CyQuant assay, HPAEC transfected with scrambled or SHH siRNA were exposed to hypoxia or normoxia for 24 h and assayed for proliferation by measuring fluorescence at 520 nm using CyQUANT® GR dye (Thermo Fisher Scientific) as per the manufacturer's protocol.

Confocal imaging

HPAEC cultured on 1% gelatin-coated chamber slides were fixed in 2% paraformaldehyde and permeabilized with 0.25% Triton X-100. After extensive washing, slides were blocked with 2% BSA solution followed by incubation with anti-Nox1, anti-NoxO1 or -p47^{phox} antibody (1:200) and subsequent incubation with FITC- or Cy3–conjugated secondary antibody (1:500), respectively (Life Technologies). Slides were adhered to glass coverslips using gelvatol mounting medium (polyvinylalcohol, glycerol, H_2O, sodium azide, and Tris; pH 8.5). Nonspecific rabbit or goat IgG (5 μg/ml) was used instead of primary antibody as a negative control. Confocal images were captured on an Olympus Fluoview 1000 confocal microscope (Olympus America Inc., Bethlehem, PA). For each experiment, 5–8 images per treatment group were captured. Three independent experiments were performed.

For immunofluorescent labeling of lung sections, 5-μm sections of antigen-retrieved, paraffin-embedded lungs were first washed using PBS and blocked in 10% BSA/PBS solution for 30 min at room temperature following permeablization. To detect specific antigens, the staining procedure was performed as described for cells.

Proximity ligation assay

Proximity ligation assay (PLA) assay was performed as described [32]. Duolink® II fluorescence assay kit (Olink Bioscience) was used according to the manufacturer's instructions. Briefly, HPAEC were seeded on 1% gelatin-coated coverslips and exposed to 1 or 21% O_2 for 24 h. Cells were fixed, permeabilized, blocked, and incubated with goat anti-Nox1 (1:500) and rabbit anti-NoxO1 (1:500) or rabbit anti-p47^{phox} (1:500) antibody overnight at 4°C. The following day, secondary antibodies conjugated with oligonucleotide PLA probes were added, ligated, and rolling-circle amplification with fluorescent oligonucleotides identified positive interaction sites as recently described [33]. Cells were counterstained with DAPI. All images were visualized and captured using an Olympus Fluoview 1000 laser scanning confocal microscope. For PLA quantitation, positive interactions indicated by green punctates in the cytoplasm were quantitated using ImageJ software (NIH, U.S.A.).

Statistics

Results are expressed as mean ± S.E.M. To compare the experimental groups, Student's *t* test or one-way ANOVA followed by Bonferroni's correction was performed using GraphPad Prism 5 software (GraphPad Software Inc., La Jolla, CA, U.S.A.). Differences with $P<0.05$ were deemed statistically significant.

Results

Nox1 and Grem1 expression and ROS levels are up-regulated in PAH patient lungs

In silico analysis suggested possible common partners between Grem1 andNox1. Importantly, two of the genes (gene products) that were identified as putative intermediaries betweem Grem1 and Nox1 also associated with pulmonary hypertension. These were tumor necrosis factor (TNF) and kinase-insert domain receptor (KDR; Supplementary Figure S1). Thus, the interactome provided promise for a potential mechanistic link amongst Nox1, Grem1, and PAH. To investigate relevance to human diseases, we explored differences in Grem1 and Nox1 expression as well as ROS in lung tissue samples from PAH and non-PAH subjects. PAH patients had mean pulmonary artery pressures (mPAP) >25 mmHg and transpulmonary pressure gradient (TPG) >12 mmHg (Table 1). Figure 1A shows that both *Nox1* and *Grem1* mRNA are significantly increased in PAH lung samples compared with non-PAH controls (3.0 ± 1.5-fold for Nox1; 6.0 ± 1.6-fold for Grem1). These mRNA increases paralleled augmentation in Nox1 and Grem1 protein (Figure 1B; 1.8 ± 0.27- and 2.0 ± 0.4-fold compared with non-PAH for Nox1 and Grem1, respectively). To localize Nox1 and Grem1, immunofluorescence was used. The intimal endothelial layer of lung blood vessels was demarcated as the region delimited circumferentially by α-smooth muscle actin staining, which stains the medial smooth muscle layer of blood vessels. This staining method was preferential as it allowed accurate identification of blood vessels and blood vessel remodeling. Figure 1C,D show increased intimal Nox1 and Grem1, respectively, in pulmonary resistance arteries (~50 μm diameter) in PAH patient lungs. We next measured ROS in PAH compared with non-PAH lung samples. Superoxide anion ($O_2^{\bullet-}$) is rapidly converted into the more stable hydrogen peroxide (H_2O_2) [26,34]. Therefore, we employed the Amplex Red assay as a means of detecting comprehensive tissue ROS levels by way of H_2O_2. Consistent with the source being Nox, the assay was performed in the presence or absence of nonspecific flavoprotein inhibitor, DPI, and addition to lung tissue homogenates of NADPH as the substrate of Nox enzymatic activity [29]. As shown in Figure 1E, a significant increase in DPI-inhibitable H_2O_2 was observed in PAH patient samples compared with controls (0.69 ± 0.06 compared with 0.43 ± 0.032 nmol/min/mg protein, respectively). To corroborate this, the cytochrome *c* assay was employed to assess $O_2^{\bullet-}$ in the rat Sugen-hypoxia (SuHx) model of occlusive, angioproliferative severe PAH, induced in female rats by a bolus injection of SU5416 (100 mg) followed by exposure to hypoxia (SuHx) [20–22]. Figure 1F shows that SuHx rat lungs display a significantly higher rate of $O_2^{\bullet-}$ production compared with normoxic controls (1.70 ± 0.07 compared with 1.33 ± 0.07 nmol/min/mg protein, respectively).

Nox1 subunit expression and assembly are increased in pulmonary ECs subjected to hypoxia

Prior studies associated Nox1 with systemic vascular reactivity, remodeling, and cell proliferation [11,33,35]. Evidence of Nox1 in the pulmonary circulation is however nonexistent. To delve into the connection between Nox1 and ROS and investigate the mechanism by which Nox1-derived ROS contribute to endothelial phenotypic switching in PAH, we utilized HPAEC subjected to hypoxia as an *in vitro* model resembling this disease. mRNA levels of canonical or hybrid Nox1 oxidase components (Nox1, NoxO1, p47^{phox}, and

NoxA1) were monitored following 6, 12, 24, 36, and 48 h hypoxia (1% O_2). *Nox1* mRNA increased in response to 24 h hypoxia (3.0 ± 0.51-fold compared with normoxic control; Figure 2A and Supplementary Figure S2). Canonical Nox1 organizer subunit *NoxO1* mRNA levels exhibited a trend toward an increase at 24 h (1.6 ± 0.27-fold, *P*=0.051; Figure 2A and Supplementary Figure S2). In contrast, there were no observed differences in Nox1 activator subunit NoxA1 or hybrid Nox1 organizer subunit *p47^{phox}* mRNA (which supplants NoxA1 in the Nox1 hybrid system). The increase in *Nox1* mRNA at 24 h correlated with an increase in Nox1 protein in response to hypoxia (Figure 2B; 1.6 ± 0.10-fold compared with normoxia). There was also a small but significant increase in NoxO1 protein (Figure 2C). Since the canonical Nox1 system is considered to be constitutively active (whereby its activity is transcriptionally regulated) whereas the hybrid system employing p47^{phox} can be activated via post-translational modifications [26,33,34], it was crucial to explore which system predominates in propagating hypoxia-induced endothelial ROS. We, therefore, examined Nox1 oxidase assembly by testing colocalization of Nox1 with either NoxO1 or p47^{phox} in HPAEC subjected to hypoxia (24 h). Nox1 and NoxO1 expression were increased by hypoxia (Figure 2D), consistent with Western blot data. Importantly, Nox1 and NoxO1 colocalization increased in response to hypoxia both in the cytosol and plasma membrane (Figure 2D), consistent with Nox1 oxidase's established presence in endosomes and caveolae [34,36]. Moreover, while confocal data suggest an increase in p47^{phox} in response to hypoxia, colocalization of Nox1 and p47^{phox} appeared weaker than that of Nox1–NoxO1 (Figure 2E).

Given these data, we tested whether the Nox1 system is the only Nox oxidase isoform up-regulated in ECs in response to hypoxia. Nox2 andNox4 have been implicated in PAH [10,37–39]. We, therefore, examined the expression ofNox2 andNox4 in HPAEC subjected to 24 h hypoxia, and in contrast with Nox1, there were no observed differences in the expression of either Nox2 or Nox4 (Supplementary Figure S3).

Since colocalization is consistent with, but does not confirm, association, we employed PLA to evaluate Nox1 oxidase subunit interaction. Figure 3 reveals that NoxO1 and p47^{phox} indeed both interact with Nox1, supporting assembly of both the canonical and hybrid oxidase systems under hypoxia, respectively. There is increased interaction in Nox1 and NoxO1 throughout the cytosol (Figure 3A) supporting previously reported Nox1's presence in endosomes [36]. Likewise, Nox1-p47^{phox} is also present, to a lesser extent, with the same localization (Figure 3B). Thus, the canonical system appears to predominate as the major assembled Nox1 oxidase in hypoxic HPAEC (Figure 3C).

Hypoxia induces Nox1-derived ROS

To test whether the increase in Nox1 oxidase expression and assembly results in increased ROS, HPAEC subjected to hypoxia (1% O_2, 24 h) were assessed for $O_2{}^{\bullet-}$ production by the cytochrome *c* assay. Figure 4A,B show a significant $O_2{}^{\bullet-}$ increase compared with normoxia (14.0 ± 1.9 compared with 6.00 ± 0.94 nmol/min/mg protein). To confirm this increase, DHE oxidation (into 2-OH-E$^+$, an indicator of intracellular $O_2{}^{\bullet-}$) using HPLC, was monitored [30]. Figure 4C,D show that hypoxia induced intracellular $O_2{}^{\bullet-}$ compared with normoxia (33 ± 5 compared with 21 ± 3 nM, respectively). To verify whether this increase in

$O_2^{\bullet-}$ was Nox1-derived, HPAEC were transfected with scrambled (Scr) or Nox1 siRNA for 24 h prior to hypoxia treatment and evaluated for $O_2^{\bullet-}$. Nox1 siRNA reduced Nox1 protein expression by over 60% (Figure 4E). Figure 4F demonstrates that Nox1 gene-silencing reduced hypoxia-induced $O_2^{\bullet-}$ production by a similar extent (31.7 ± 2.5 compared with 19.4 ± 1.6 nmol/min/mg protein for Scr compared with Nox1 siRNA hypoxia groups, respectively).

Hypoxia induces Nox1-mediated Grem1 and SHH expression

To interrogate a link between Nox1-derived ROS and Grem1, we first tested whether Grem1 expression is up-regulated in pulmonary ECs. HPAEC were subjected to hypoxia and *Grem1* mRNA and protein were quantitated. Figure 5A shows that *Grem1* mRNA is significantly up-regulated by hypoxia (3.0 ± 0.024-fold compared with normoxia). This was accompanied by a significant increase in Grem1 protein by both Western blot (1.90 ± 0.32-fold relative compared with normoxia; Figure 5B) and confocal microscopy (Supplementary Figure S4). This up-regulation coincides with the time dependence of Nox1 expression, assembly, and ROS production in response to hypoxia. Thus, we tested a causal link by investigating whether the increase in Grem1 expression is Nox1 dependent. HPAEC were transfected with Nox1 or Scr siRNA and evaluated for Grem1 protein. Figure 5C shows that Nox1 knockdown abolished hypoxia-induced Grem1, revealing for the first time that hypoxia-induced Nox1 activation up-regulates Grem1 expression in pulmonary ECs.

To gain greater insight into the effector of Nox1-derived ROS on Grem1 expression, we investigated a possible involvement of SHH. We focussed on this pathway as it is a key driver of cellular pattern formation, differentiation, and proliferation [19,40], and has been implicated in arterial remodeling [41]. First, we explored whether SHH is differentially expressed in lung tissue samples from PAH and non-PAH subjects. Western blot data (Supplementary Figure S5) show that SHH is increased in PAH lung samples compared with non-PAH controls (2.5 ± 0.7-fold). Despite being very close, these data, however, did not reach statistical significance, likely owing to human tissue variability (P=0.0515). HPAEC were transfected with Nox1 or scrambled siRNA and subjected to hypoxia (24 h). Figure 5D shows that hypoxia induced SHH expression (1.5 ± 0.011-fold compared with normoxic control). Importantly, Nox1 gene-silencing abolished this increase (Figure 5D), supporting aNox1-dependent activation of SHH signaling, an upstream modulator of Grem1 [42–44]. To further support that Nox1-derived ROS activates SHH, we treated HPAEC exogenously with varying concentrations of H_2O_2. H_2O_2 treatment (100 μM, 4 h) resulted in a significant increase in SHH expression (Supplementary Figure S6). Finally, to test whether SHH is causally linked to Grem1 expression and pulmonary EC proliferation, SHH siRNA was transfected into HPAEC and subjected to normoxia or hypoxia. Supplementary Figure S7 shows that SHH siRNA abolished hypoxia-induced Grem1 expression and HPAEC proliferation, supporting activation of a Nox1-SHH-Grem1 pro-proliferative pathway under endothelial hypoxic stress.

Hypoxia elicits pulmonary EC proliferation in Nox1- and Grem1-dependent manner

Grem1 is a BMP receptor antagonist that can act in an autocrine fashion to inhibit BMP signaling, leading to proliferation [12,13,15,16,45]. To investigate whether the increase in

Nox1 and attendant increase in Grem1 results in a proliferative response, HPAEC were transfected with Nox1 or scrambled siRNA, subjected to 24 h hypoxia and cellular proliferation assessed by BrdU incorporation [46]. A significant increase in HPAEC BrdU incorporation was found following hypoxia (1.18 ± 0.038-fold relative to normoxic control), a response that was abolished by Nox1 siRNA (Figure 6A). To test the putative role of Grem1, hypoxia-induced HPAEC proliferation was quantitated using CFSE fluorescence by FACS after transfection with Grem1 or scrambled siRNA. Figure 6B shows that hypoxia induced a significant increase in the number of proliferating cells compared with normoxia ($4.6 \pm 1.4\%$ compared with 1.0% of total cells, respectively). Importantly, gene silencing of Grem1 abolished hypoxia-induced proliferation (Figure 6B,C).

Discussion

The mechanisms responsible for pulmonary vascular endothelial proliferation in PAH remain poorly understood. The major findings of the current study culminate in the discovery of a Nox1-instigated cellular process that drives proliferation via SHH and Grem1 in the pulmonary endothelium. This pathway was activated in lungs from PAH patients, supporting its clinical significance. The oxidase capacity of Nox1 in the PAH endothelium is activated through assembly of both the canonical and hybrid Nox1 systems. These elicit an increase in Nox1-derived ROS and subsequent up-regulation of SHH and Grem1 expression, as revealed by changes in protein expression. Grem1 release ensues and leads to an increase in pulmonary endothelial proliferation (Figure 7).

Our data on Nox1 expression and assembly reveal critical new information on how this enzyme functions in the pulmonary endothelium and, to our knowledge, ECs in general. Multiple lines of evidence support an increase in Nox1 and, to a lesser extent NoxO1, expression in PAH. We show by qPCR, Western blotting, and confocal microscopy an increase in Nox1 expression both in PAH patients' lungs and isolated HPAEC subjected to hypoxia. We also show by confocal imaging and the PLA assay increased assembly of the canonical (involving NoxO1) and hybrid (involving p47^{phox}) Nox1 systems in hypoxic ECs. Activation of NoxO1 is thought to be regulated through expression and NoxO1 participation in Nox1 oxidase activity occurs via a constitutive association with Nox1 yielding a constitutively assembled and active Nox1 oxidase system [34]. This is in contrast with p47^{phox}, which is widely accepted to be activated upon phosphorylation, causing conformational changes that expose Nox-binding domains [33,34]. The observation that both canonical and hybrid Nox1 systems are activated in EC under the same stimulus (hypoxia in the current study) suggest a dual mode of Nox1 activation during PAH. Since p47^{phox} phosphorylation is necessary for its membrane translocation and association with catalytic subunits, one mode of Nox1 oxidase activation in these cells could be an acute response that involves increased assembly and activation of pre-existent subunits of the enzyme. The other mode could be a more chronic adaptation and involve increased expression of Nox1 and NoxO1. Further experimentation would be necessary, however, to support this notion of an acute compared with chronic response during PAH and to test whether these responses could underlie events of PAH initiation and prolongation, respectively. The observed increase in ROS in human PAH lungs, rat SuHx lungs, and cultured ECs exposed to hypoxia (confirmed by three independent and robust detection

methods) and attenuation of this increase by *Nox1* gene silencing further support Nox1's role in PAH.

Despite the fact that EC proliferation is crucial for initiation and progression of severe pulmonary hypertension [47], the mechanisms driving this process are not well understood. Our data demonstrate that *Grem1* mRNA and protein are increased in PAH patient lungs as well as in hypoxic HPAEC. We also demonstrate that loss of Grem1 attenuates hypoxia-induced EC proliferation. These data are consistent with the previous findings of a role forGrem1 in vascular remodeling in PAH [14,16–18,45]. Importantly, we expand significantly on previous discoveries by demonstrating a heretofore unknown Nox1-dependent regulation of Grem1. Our findings demonstrate that Nox1 gene silencing attenuates hypoxia-induced Grem1 protein expression and EC proliferation and support a Nox1–Grem1 causal relationship that contributes to the PAH vascular phenotype. Further insight into this signaling pathway is gained by data demonstrating for the first time that Nox1 gene-silencing attenuates hypoxia-induced SHH expression. These findings built upon previous reports supporting that SHH is up-regulated in response to oxidative stress [48,49] and associated with cell proliferation and arterial remodeling [40,41]. Previous studies have also demonstrated that Grem1 is downstream of SHH signaling [42–44]. Indeed, our current data demonstrated that in ECs, SHH is up-regulated in response to Nox1 oxidase activation and in response to exogenous H_2O_2; and support up-regulation of SHH in PAH patients. We also showed that SHH is upstream of Grem1 expression and pulmonary EC proliferation following hypoxic insult. In aggregate, our findings support a mechanism whereby SHH is an intermediary between hypoxia-induced Nox1-derived ROS and Grem1 and, in turn, endothelial proliferation.

Definitive identification ofNox1's role as an upstream modulator ofGrem1 in the pulmonary endothelium appears to quell some of the controversy confounding a role for various Nox isoforms in PAH-associated vascular remodeling [50–54]. Careful consideration of this literature reveals that Nox isoforms in PAH are likely to play cell-specific roles in the disease. Our current data unveil a unique role for Nox1 in endothelial proliferation in PAH. Therapeutic implications of the Nox1–Grem1 pathway are brought to the forefront by our human tissue and rat PAH data.

Taken together, the findings of the current study identify a novel signaling axis in PAH in which pulmonary vascular endothelial Nox1 is activated, leading to an increase in ROS, SHH, and a subsequent increase in Grem1 expression. The rise in Grem1 drives an increase in endothelial proliferation that contributes to the pathogenesis of PAH. These findings were supported by data collected from human tissues, underscoring clinical relevance of this new signaling pathway, and identifying the Nox1–Grem1 axis as a potential new target for multipronged therapeutic strategies.

Supplementary Material

Refer to Web version on PubMed Central for supplementary material.

Author Manuscript

Author Manuscript

Author Manuscript

Author Manuscript

Acknowledgments

We thank Dr. Claudette St. Croix and members of the Center for Biologic Imaging at the University of Pittsburgh for their guidance and access to confocal resources.

Abbreviations

BMP	bone morphogenetic protein
CFSE	carboxyfluorescein succinimidyl ester
DHE	dihydroethidium
DPI	diphenylene iodonium
EC	endothelial cell
Grem1	Gremlin1
HPAEC	human pulmonary artery endothelial cell
Nox1	NADPH oxidase 1
NoxA1	Nox activator 1
NoxO1	Nox organizer 1
PAH	pulmonary arterial hypertension
PLA	proximity ligation assay
PVR	pulmonary vascular resistance
RV	right ventricle
ROS	reactive oxygen species
SHH	sonic hedgehog
SOD	superoxide dismutase
SuHx	Sugen-hypoxia
SU5416	Sugen

References

1. McLaughlin VV, Archer SL, Badesch DB, Barst RJ, Farber HW, Lindner JR, et al. ACCF/AHA 2009 expert consensus document on pulmonary hypertension a report of the American College of Cardiology Foundation Task Force on Expert Consensus Documents and the American Heart

Association developed in collaboration with the American College of Chest Physicians; American Thoracic Society, Inc.; and the Pulmonary Hypertension Association. J. Am. Coll. Cardiol. 2009; 53:1573–1619. [PubMed: 19389575]

2. Benza RL, Miller DP, Barst RJ, Badesch DB, Frost AE, McGoon MD. An evaluation of long-term survival from time of diagnosis in pulmonary arterial hypertension from the REVEAL Registry. Chest. 2012; 142:448–456. [PubMed: 22281797]

3. Cool CD, Groshong SD, Oakey J, Voelkel NF. Pulmonary hypertension: cellular and molecular mechanisms. Chest. 2005; 128:565S–571S. [PubMed: 16373828]

4. Rabinovitch M. Molecular pathogenesis of pulmonary arterial hypertension. J. Clin. Invest. 2012; 122:4306–4313. [PubMed: 23202738]

5. Tuder RM, Chacon M, Alger L, Wang J, Taraseviciene-Stewart L, Kasahara Y, et al. Expression of angiogenesis-related molecules in plexiform lesions in severe pulmonary hypertension: evidence for a process of disordered angiogenesis. J. Pathol. 2001; 195:367–374. [PubMed: 11673836]

6. Tuder RM, Groves B, Badesch DB, Voelkel NF. Exuberant endothelial cell growth and elements of inflammation are present in plexiform lesions of pulmonary hypertension. Am. J. Pathol. 1994; 144:275–285. [PubMed: 7508683]

7. Lee SD, Shroyer KR, Markham NE, Cool CD, Voelkel NF, Tuder RM. Monoclonal endothelial cell proliferation is present in primary but not secondary pulmonary hypertension. J. Clin. Invest. 1998; 101:927–934. [PubMed: 9486960]

8. Masri FA, Xu W, Comhair SA, Asosingh K, Koo M, Vasanji A, et al. Hyperproliferative apoptosis-resistant endothelial cells in idiopathic pulmonary arterial hypertension. Am. J. Physiol. Lung Cell. Mol. Physiol. 2007; 293:L548–L554. [PubMed: 17526595]

9. Bowers R, Cool C, Murphy RC, Tuder RM, Hopken MW, Flores SC, et al. Oxidative stress in severe pulmonary hypertension. Am. J. Respir. Crit. Care Med. 2004; 169:764–769. [PubMed: 14701708]

10. Fresquet F, Pourageaud F, Leblais V, Brandes RP, Savineau JP, Marthan R, et al. Role of reactive oxygen species and gp91phox in endothelial dysfunction of pulmonary arteries induced by chronic hypoxia. Br. J. Pharmacol. 2006; 148:714–723. [PubMed: 16715116]

11. Lassegue B, San Martin A, Griendling KK. Biochemistry, physiology, and pathophysiology of NADPH oxidases in the cardiovascular system. Circ. Res. 2012; 110:1364–1390. [PubMed: 22581922]

12. Hsu DR, Economides AN, Wang X, Eimon PM, Harland RM. The Xenopus dorsalizing factor Gremlin identifies a novel family of secreted proteins that antagonize BMP activities. Mol. Cell. 1998; 1:673–683. [PubMed: 9660951]

13. Shi W, Zhao J, Anderson KD, Warburton D. Gremlin negatively modulates BMP-4 induction of embryonic mouse lung branching morphogenesis. Am. J. Physiol. Lung Cell. Mol. Physiol. 2001; 280:L1030–L1039. [PubMed: 11290528]

14. Stabile H, Mitola S, Moroni E, Belleri M, Nicoli S, Coltrini D, et al. Bone morphogenic protein antagonist Drm/gremlin is a novel proangiogenic factor. Blood. 2007; 109:1834–1840. [PubMed: 17077323]

15. Sun J, Zhuang FF, Mullersman JE, Chen H, Robertson EJ, Warburton D, et al. BMP4 activation and secretion are negatively regulated by an intracellular gremlin-BMP4 interaction. J. Biol. Chem. 2006; 281:29349–29356. [PubMed: 16880207]

16. Costello CM, Cahill E, Martin F, Gaine S, McLoughlin P. Role of gremlin in the lung: development and disease. Am. J. Respir. Cell. Mol. Biol. 2010; 42:517–523. [PubMed: 19574532]

17. Kim M, Yoon S, Lee S, Ha SA, Kim HK, Kim JW, et al. Gremlin-1 induces BMP-independent tumor cell proliferation, migration, and invasion. PLoS ONE. 2012; 7:e35100. [PubMed: 22514712]

18. Maciel TT, Melo RS, Schor N, Campos AH. Gremlin promotes vascular smooth muscle cell proliferation and migration. J. Mol. Cell. Cardiol. 2008; 44:370–379. [PubMed: 18086474]

19. Byrd N, Becker S, Maye P, Narasimhaiah R, St-Jacques B, Zhang X, et al. Hedgehog is required for murine yolk sac angiogenesis. Development. 2002; 129:361–372. [PubMed: 11807029]

20. Rafikova O, Rafikov R, Kumar S, Sharma S, Aggarwal S, Schneider F, et al. Bosentan inhibits oxidative and nitrosative stress and rescues occlusive pulmonaryhypertension. Free Radic. Biol. Med. 2013; 56:28–43. [PubMed: 23200808]

21. Gomez-Arroyo J, Mizuno S, Szczepanek K, Van Tassell B, Natarajan R, dos Remedios CG, et al. Metabolic gene remodeling and mitochondrial dysfunction in failing right ventricular hypertrophy secondary to pulmonary arterial hypertension. Circ. Heart Fail. 2013; 6:136–144. [PubMed: 23152488]

22. Taraseviciene-Stewart L, Kasahara Y, Alger L, Hirth P, Mc Mahon G, Waltenberger J, et al. Inhibition of the VEGF receptor 2 combined with chronic hypoxia causes cell death-dependent pulmonary endothelial cell proliferation and severe pulmonary hypertension. FASEB J. 2001; 15:427–438. [PubMed: 11156958]

23. Toby IT, Chicoine LG, Cui H, Chen B, Nelin LD. Hypoxia-induced proliferation of human pulmonary microvascular endothelial cells depends on epidermal growth factor receptor tyrosine kinase activation. Am. J. Physiol. Lung Cell. Mol. Physiol. 2010; 298:L600–L606. [PubMed: 20139181]

24. Han Y, Yang K, Proweller A, Zhou G, Jain MK, Ramirez-Bergeron DL. Inhibition of ARNT severely compromises endothelial cell viability and function in response to moderate hypoxia. Angiogenesis. 2012; 15:409–420. [PubMed: 22484908]

25. Gammella E, Leuenberger C, Gassmann M, Ostergaard L. Evidence of synergistic/additive effects of sildenafil and erythropoietin in enhancing survival and migration of hypoxic endothelial cells. Am. J. Physiol. Lung Cell. Mol. Physiol. 2013; 304:L230–L239. [PubMed: 23204066]

26. Al Ghouleh I, Frazziano G, Rodriguez AI, Csanyi G, Maniar S, St Croix CM, et al. Aquaporin 1, Nox1, and Ask1 mediate oxidant-induced smooth muscle cell hypertrophy. Cardiovasc. Res. 2013; 97:134–142. [PubMed: 22997161]

27. Frazziano G, Al Ghouleh I, Baust J, Shiva S, Champion HC, Pagano PJ. Nox-derived ROS are acutely activated in pressure overload pulmonary hypertension: indications for a seminal role for mitochondrial Nox4. Am. J. Physiol. Heart Circ. Physiol. 2014; 306:H197–H205. [PubMed: 24213612]

28. Al Ghouleh I, Rodriguez A, Pagano PJ, Csanyi G. Proteomic analysis identifies an NADPH oxidase 1 (Nox1)-mediated role for actin-related protein 2/3 complex subunit 2 (ARPC2) in promoting smooth muscle cell migration. Int. J. Mol. Sci. 2013; 14:20220–20235. [PubMed: 24152438]

29. Csanyi G, Cifuentes-Pagano E, Al Ghouleh I, Ranayhossaini DJ, Egana L, Lopes LR, et al. Nox2 B-loop peptide, Nox2ds, specifically inhibits the NADPH oxidase Nox2. Free Radic. Biol. Med. 2011; 51:1116–1125. [PubMed: 21586323]

30. Zielonka J, Vasquez-Vivar J, Kalyanaraman B. Detection of 2-hydroxyethidium in cellular systems: a unique marker product of superoxide and hydroethidine. Nat. Protoc. 2008; 3:8–21. [PubMed: 18193017]

31. Csanyi G, Yao M, Rodriguez AI, Al Ghouleh I, Sharifi-Sanjani M, Frazziano G, et al. Thrombospondin-1 regulates blood flow via CD47 receptor-mediated activation of NADPH oxidase 1. Arterioscler. Thromb. Vasc. Biol. 2012; 32:2966–2973. [PubMed: 23087362]

32. Soderberg O, Gullberg M, Jarvius M, Ridderstrale K, Leuchowius KJ, Jarvius J, et al. Direct observation of individual endogenous protein complexes *in situ* by proximity ligation. Nat. Methods. 2006; 3:995–1000. [PubMed: 17072308]

33. Al Ghouleh I, Meijles DN, Mutchler S, Zhang Q, Sahoo S, Gorelova A, et al. Binding of EBP50 to Nox organizing subunit p47phox is pivotal to cellular reactive species generation and altered vascular phenotype. Proc. Natl. Acad. Sci. U.S.A. 2016; 113:E5308–E5317. [PubMed: 27540115]

34. Al Ghouleh I, Khoo NKH, Knaus UG, Griendling KK, Touyz RM, Thannickal VJ, et al. Oxidases and peroxidases in cardiovascular and lung disease: new concepts in reactive oxygen species signaling. Free Radic. Biol. Med. 2011; 51:1271–1288. [PubMed: 21722728]

35. Lee MY, San Martin A, Mehta PK, Dikalova AE, Garrido AM, Datla SR, et al. Mechanisms of vascular smooth muscle NADPH oxidase 1 (Nox1) contribution to injury-induced neointimal formation. Arterioscler. Thromb. Vasc. Biol. 2009; 29:480–487. [PubMed: 19150879]

36. Chu X, Filali M, Stanic B, Takapoo M, Sheehan A, Bhalla R, et al. A critical role for chloride channel-3 (CIC-3) in smooth muscle cell activation and neointima formation. Arterioscler. Thromb. Vasc. Biol. 2011; 31:345–351. [PubMed: 21071705]

37. Liu Y, Hao W, Letiembre M, Walter S, Kulanga M, Neumann H, et al. Suppression of microglial inflammatory activity by myelin phagocytosis: role of p47-PHOX-mediated generation of reactive oxygen species. J. Neurosci. 2006; 26:12904–12913. [PubMed: 17167081]

38. Mittal M, Roth M, Konig P, Hofmann S, Dony E, Goyal P, et al. Hypoxia-dependent regulation of nonphagocytic NADPH oxidase subunit NOX4 in the pulmonary vasculature. Circ. Res. 2007; 101:258–267. [PubMed: 17585072]

39. Veith C, Kraut S, Wilhelm J, Sommer N, Quanz K, Seeger W, et al. NADPH oxidase 4 is not involved in hypoxia-induced pulmonary hypertension. Pulm. Circ. 2016; 6:397–400. [PubMed: 27683617]

40. Wang G, Zhang Z, Xu Z, Yin H, Bai L, Ma Z, et al. Activation of the sonic hedgehog signaling controls human pulmonary arterial smooth muscle cell proliferation in response to hypoxia. Biochim. Biophys. Acta. 2010; 1803:1359–1367. [PubMed: 20840857]

41. Morrow D, Sweeney C, Birney YA, Guha S, Collins N, Cummins PM, et al. Biomechanical regulation of hedgehog signaling in vascular smooth muscle cells *in vitro* and *in vivo*. Am. J. Physiol. Cell Physiol. 2007; 292:C488–C496. [PubMed: 16943241]

42. Zuniga A, Haramis AP, McMahon AP, Zeller R. Signal relay by BMP antagonism controls the SHH/FGF4 feedback loop in vertebrate limb buds. Nature. 1999; 401:598–602. [PubMed: 10524628]

43. Khokha MK, Hsu D, Brunet LJ, Dionne MS, Harland RM. Gremlin is the BMP antagonist required for maintenance of Shh and Fgf signals during limb patterning. Nat. Genet. 2003; 34:303–307. [PubMed: 12808456]

44. Michos O, Panman L, Vintersten K, Beier K, Zeller R, Zuniga A. Gremlin-mediated BMP antagonism induces the epithelial-mesenchymal feedback signaling controlling metanephric kidney and limb organogenesis. Development. 2004; 131:3401–3410. [PubMed: 15201225]

45. Cahill E, Costello CM, Rowan SC, Harkin S, Howell K, Leonard MO, et al. Gremlin plays a key role in the pathogenesis of pulmonary hypertension. Circulation. 2012; 125:920–930. [PubMed: 22247494]

46. Messele T, Roos MT, Hamann D, Koot M, Fontanet AL, Miedema F, et al. Nonradioactive techniques for measurement of *in vitro* T-cell proliferation: alternatives to the [(3)H]thymidine incorporation assay. Clin. Diagn. Lab. Immunol. 2000; 7:687–692. [PubMed: 10882673]

47. Tuder RM, Cool CD, Yeager M, Taraseviciene-Stewart L, Bull TM, Voelkel NF. The pathobiology of pulmonary hypertension. Endothelium. Clin. Chest Med. 2001; 22:405–418. [PubMed: 11590837]

48. Dai RL, Zhu SY, Xia YP, Mao L, Mei YW, Yao YF, et al. Sonic hedgehog protects cortical neurons against oxidative stress. Neurochem. Res. 2011; 36:67–75. [PubMed: 20848190]

49. Xia YP, Dai RL, Li YN, Mao L, Xue YM, He QW, et al. The protective effect of sonic hedgehog is mediated by the phosphoinositide [corrected] 3-kinase/AKT/Bcl-2 pathway in cultured rat astrocytes under oxidative stress. Neuroscience. 2012; 209:1–11. [PubMed: 22402346]

50. Veit F, Pak O, Egemnazarov B, Roth M, Kosanovic D, Seimetz M, et al. Function of NADPH oxidase 1 in pulmonary arterial smooth muscle cells after monocrotaline-induced pulmonary vascular remodeling. Antioxid. Redox Signal. 2013; 19:2213–2231. [PubMed: 23706097]

51. Dennis KE, Aschner JL, Milatovic D, Schmidt JW, Aschner M, Kaplowitz MR, et al. NADPH oxidases and reactive oxygen species at different stages of chronic hypoxia-induced pulmonary hypertension in newborn piglets. Am. J. Physiol. Lung Cell. Mol. Physiol. 2009; 297:L596–L607. [PubMed: 19592458]

52. Green DE, Murphy TC, Kang BY, Kleinhenz JM, Szyndralewiez C, Page P, et al. The Nox4 inhibitor GKT137831 attenuates hypoxia-induced pulmonary vascular cell proliferation. Am. J. Respir. Cell. Mol. Biol. 2012; 47:718–726. [PubMed: 22904198]

53. Chen F, Barman S, Yu Y, Haigh S, Wang Y, Black SM, et al. Caveolin-1 is a negative regulator of NADPH oxidase-derived reactive oxygen species. Free Radic. Biol. Med. 2014; 73:201–213. [PubMed: 24835767]

54. Iwata K, Ikami K, Matsuno K, Yamashita T, Shiba D, Ibi M, et al. Deficiency of NOX1/nicotinamide adenine dinucleotide phosphate, reduced form oxidase leads to pulmonary vascular remodeling. Arterioscler. Thromb. Vasc. Biol. 2014; 34:110–119. [PubMed: 24233492]

Clinical perspectives

- PAH is a rapidly degenerating disease that leads to death from right heart failure. Despite the availability of a number of FDA-approved drugs, prognosis remains poor, largely attributed to limited understanding of mechanisms driving the underlying vascular remodeling. While endothelial proliferation is considered by many to propagate pathological remodeling of the pulmonary vasculature, little is known about how the pulmonary endothelium is regulated in PAH.

- Our current findings demonstrate up-regulation of Nox1, Grem1, and ROS in human PAH lungs and hypoxia-exposed human pulmonary ECs. We report a novel signaling pathway whereby Nox1 drives SHH and Grem1 induction and leads to pulmonary EC proliferation.

- This new signaling axis has broad implications on the angioproliferative and vasculo-occlusive processes driving PAH in patients and may serve as a promising therapeutic target for future development of new classes of anti-PAH drug.
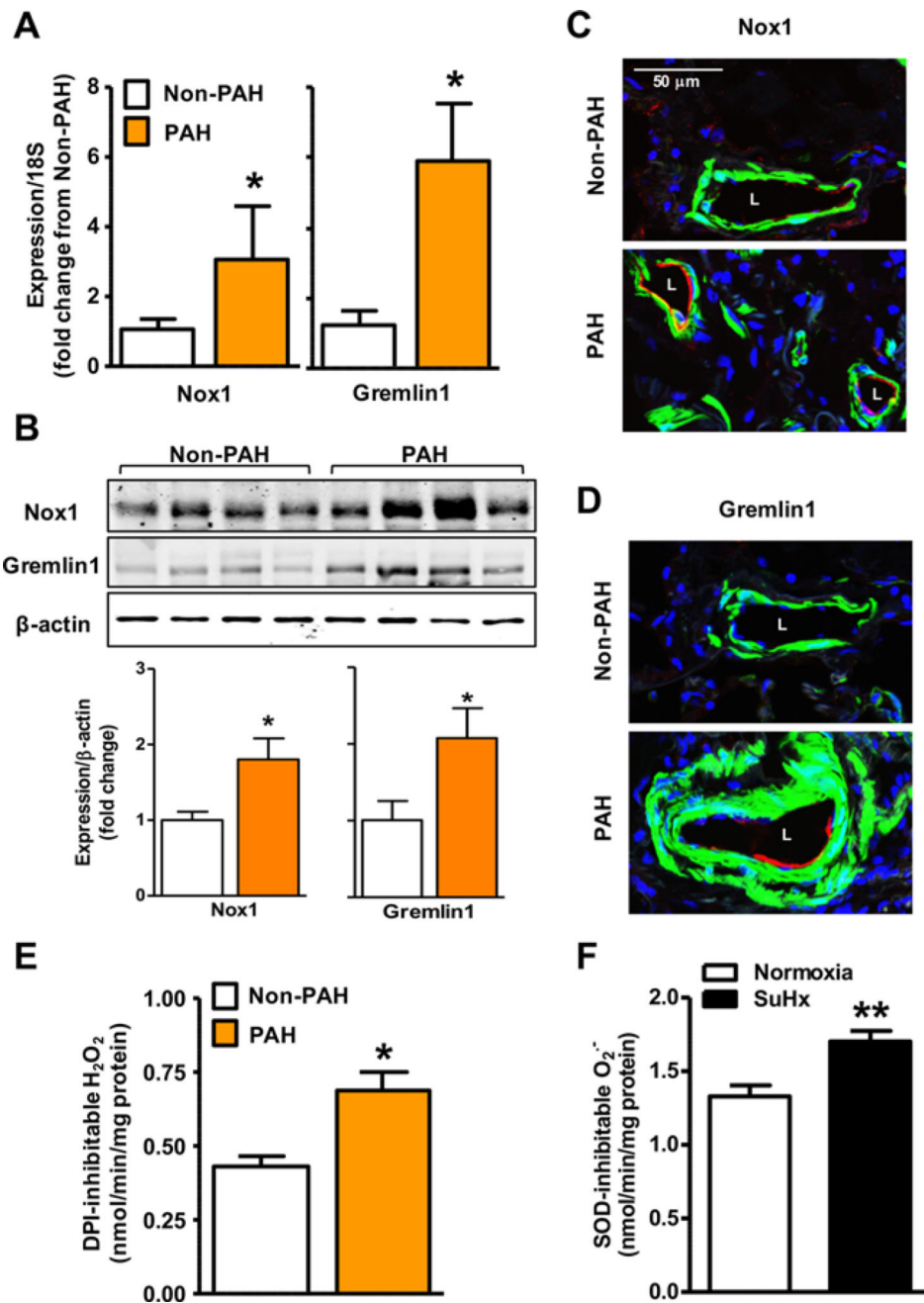
Figure 1. Human PAH is associated with increased Nox1 and Grem1 expression and elevated ROS production that is paralleled in rat PAH

(**A**) Real-time qPCR analysis of *Nox1* and *Grem1* mRNA levels normalized to 18S in lung tissue samples from patients with PAH compared with non-PAH controls (*n*=3–5). (**B**) Western blot analysis of Nox1, Grem1, and β-actin protein levels in lung tissue samples from patients with PAH compared with non-PAH controls. Bar graph shows densitometry quantitation of protein expression normalized to β-actin protein expression (*n*=7–9). (**C**,**D**) Expression of Nox1 (C, red) and Grem1 (D, red) in PAH and non-PAH human lung sections by co-immunofluorescent staining. Sections were counterstained with α-smooth muscle

actin (green) to visualize the medial smooth muscle layer of blood vessels, and DAPI (blue) to visualize the nuclei; the endothelial layer (intima) was defined as the layer delimited circumferentially by α-smooth muscle actin staining; L refers to vessel lumen. Scale bars represent 50 μm. (**E**) Increased DPI-inhibitable total homogenate comprehensive tissue ROS levels (direct H_2O_2 production plus dismuted $O_2^{\bullet-}$) in lungs of PAH patients compared with non-PAH controls as measured by Amplex Red fluorescence for evaluation of H_2O_2 (n=4). *P<0.05 compared with non-PAH by Student's t test. (**F**) Increased $O_2^{\bullet-}$ in total lung homogenates of SuHx-treated rats compared with normoxia-treated controls measured by the cytochrome c reduction assay. **P<0.01 compared with normoxia (n=5). The results are means ± S.E.M. of indicated sample size.
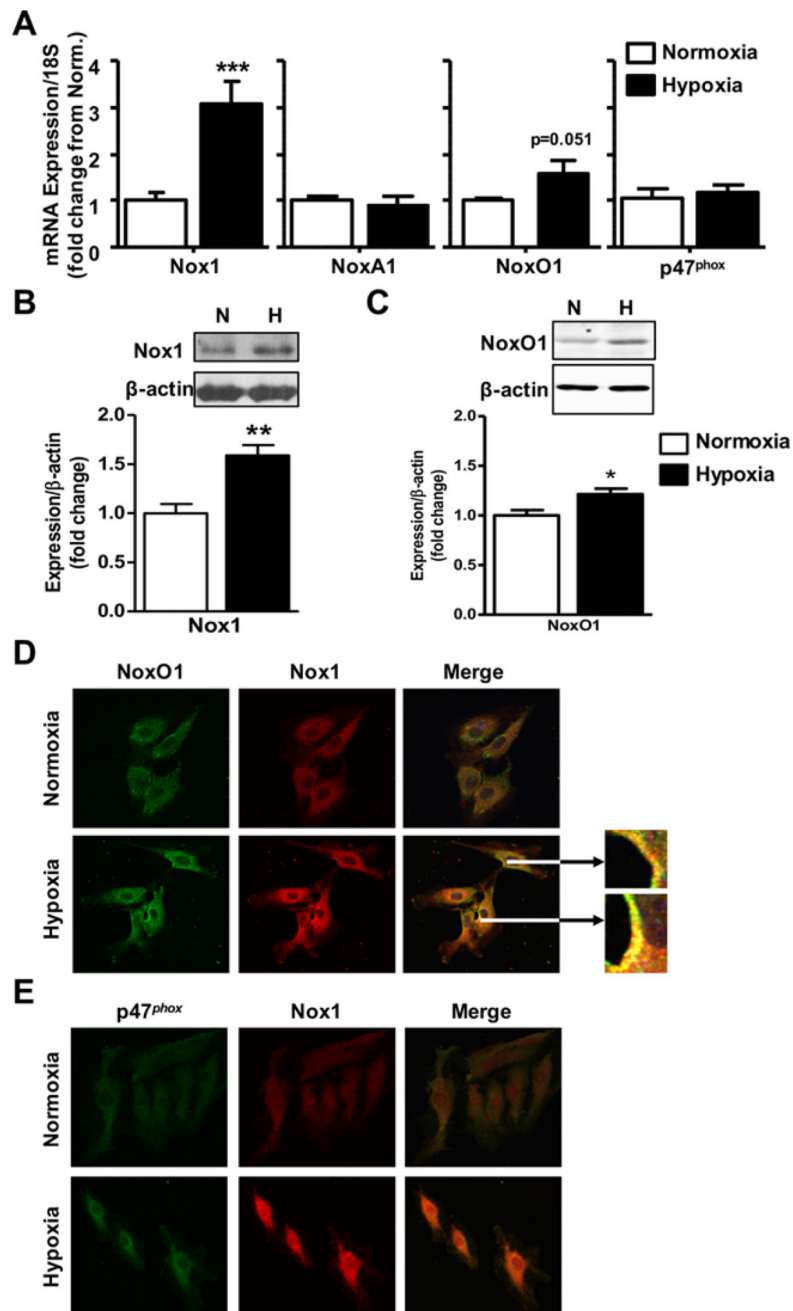
Figure 2. Hypoxia increases expression of Nox1 oxidase and its subunits in HPAEC

(**A**) Analysis by qPCR of *Nox1, NoxA1, NoxO1*, and *p47^{phox}* mRNA levels normalized to 18S in HPAEC in response to 24 h of hypoxia depicted as fold from normoxic control (*n*=3–6). (**B,C**) Western blot analysis of Nox1 and NoxO1 protein levels in response to 24 h of hypoxia in HPAEC; bar graphs depict densitometry quantitation normalized to β-actin (*n*=6–8). *$P<0.05$; **$P<0.01$; ***$P<0.001$ compared with normoxia by Student's *t* test. (**D,E**) Confocal immunofluorescence images of Nox1 showing increased expression and colocalization with NoxO1 and p47^{phox} following 24 h hypoxia in HPAEC. HPAEC were

double immunostained for NoxO1 (green, D) or p47^{phox} (green, E), and Nox1 (red, D and E). Inset shows magnification of areas of colocalization; n=3.

Author Manuscript
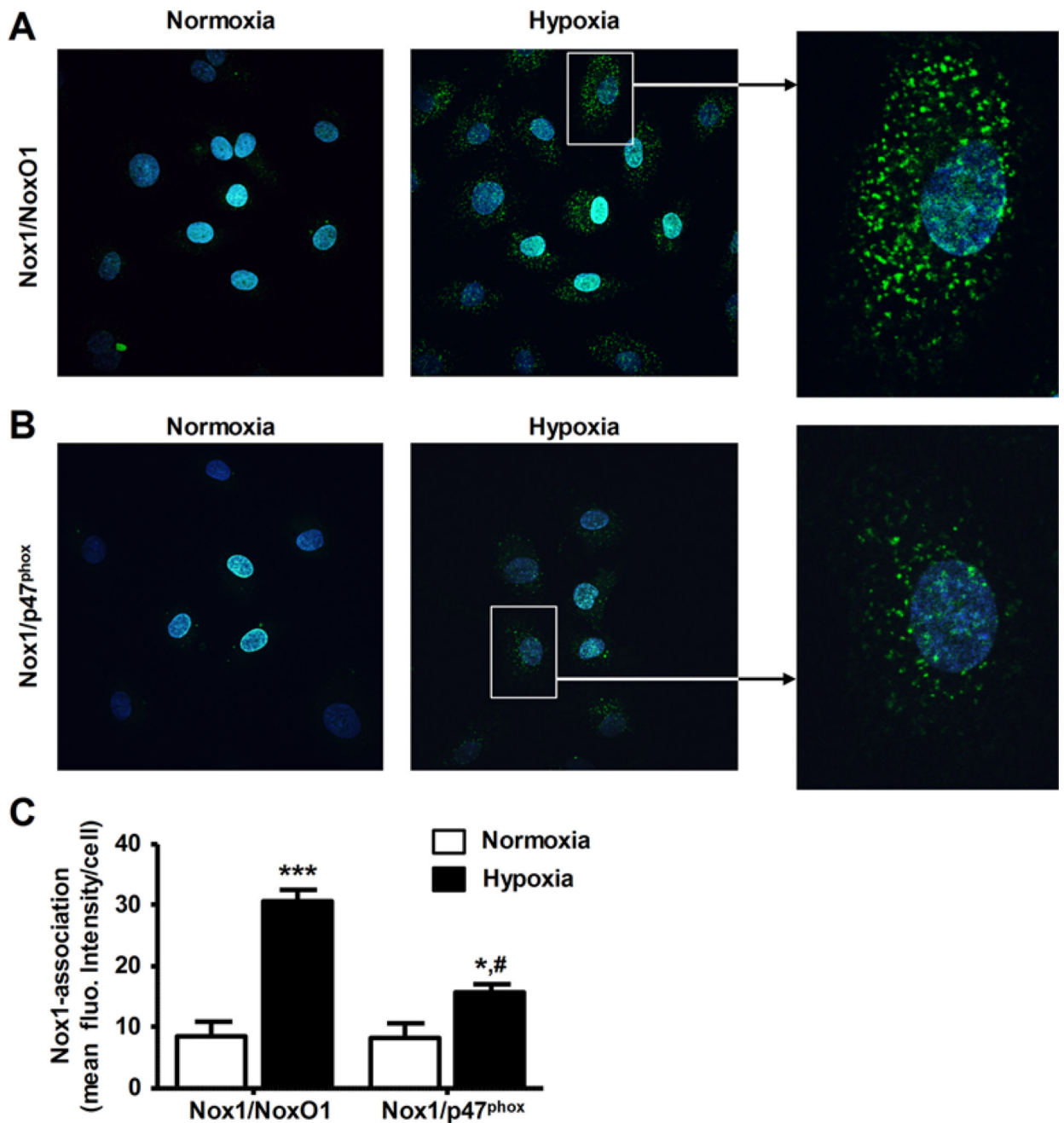Author Manuscript
Author Manuscript
Author Manuscript

Figure 3. Hypoxia increases binding of Nox1 oxidase subunits in HPAEC

(**A,B**) PLA for Nox1 and p47^{phox} or Nox1 and NoxO1 (green punctates) following 24 h hypoxia in HPAEC. Nuclei were stained with DAPI (blue). (**C**) Quantitation of PLA results from A and B (*n*=3). *$P<0.05$; ***$P<0.001$ compared with normoxia; #$P<0.05$ compared with Nox1–NoxO1 interaction in hypoxia.
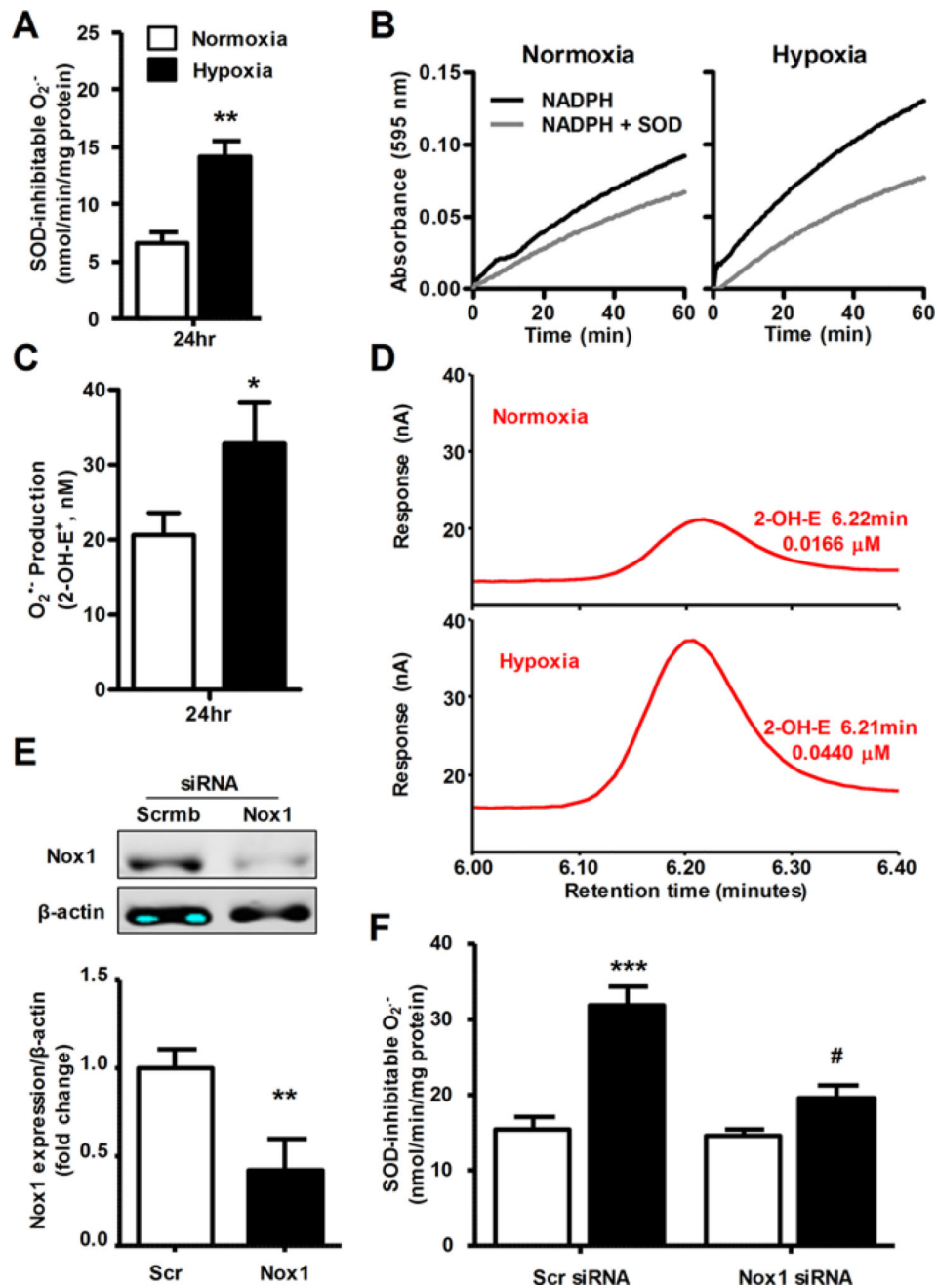
Figure 4. Hypoxia induces ROS in HPAEC, which is attenuated by Nox1 silencing

(**A**) Membrane fractions were prepared from HPAEC exposed to normoxia or hypoxia for the indicated times and assayed for $O_2^{\bullet-}$ levels by cytochrome c reduction assay (n=6); **P<0.01 compared with normoxia. (**B**) Representative cytochrome c absorbance over time plots. (**C**) HPAEC were exposed to hypoxia for 24 h and pretreated for 30 min with 10 μM DHE prior to lysis. Evaluation of $O_2^{\bullet-}$ levels was made using DHE-HPLC assay (n=5); *P<0.05 compared with normoxia. (**D**) Representative HPLC retention time plot. Values on plot indicate retention times and concentrations of 2-OH-E+ for one representative plot (**E**)Western blot analysis of Nox1 in HPAEC following transfection with scrambled (Scr) or

Nox1 siRNA (n=3); **P<0.01 compared with Scr. (**F**) HPAEC transfected with scrambled (Scr) or Nox1 siRNA were exposed to hypoxia for 24 h, and then assayed for $O_2^{\bullet-}$ levels by cytochrome c reduction assay using membrane fractions (n=9); ***P<0.001 compared with Scr normoxia, [#]P<0.05 compared with Scr hypoxia by one-way ANOVA.
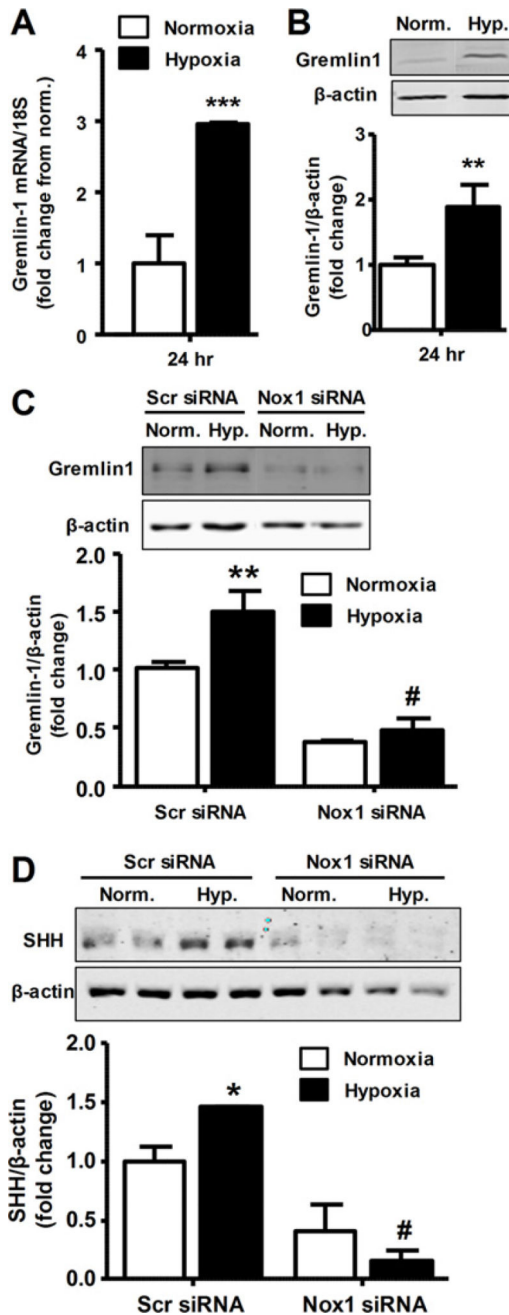
Figure 5. Hypoxia induces Nox1-dependent Grem1 expression in HPAEC
(**A**) Real-time qPCR analysis of *Grem1* mRNA expression normalized to 18S in HPAEC subjected to hypoxia for the indicated times shown as fold from respective normoxic controls (*n*=6). (**B**) HPAEC were exposed to hypoxia for 24 h and then lysed and subjected to Western blotting for Grem1 and β-actin. Bar graph shows absorbance quantitation normalized to β-actin and depicted as fold from normoxia (*n*=6). (**C**) HPAEC transfected with Nox1 siRNA or scrambled siRNA (Scr) were exposed to hypoxia for 24 h, and then lysed and subjected to Western blotting for Grem1 and β-actin. Bar graph shows absorbance quantitation normalized to β-actin and depicted as fold from Scr normoxia control (*n*=6).

(**D**) Western blot analysis of SHH expression in HPAEC transfected with Nox1 siRNA (siRNA) or scrambled control siRNA (Scr) and subjected to 24 h hypoxia; bar graph shows absorbance quantitation normalized to β-actin and depicted as fold from Scr normoxia control (*n*=3). ***P<0.001 compared with normoxia, **P<0.01 compared with respective normoxia group, #*P*<0.01 compared with Scr hypoxia, *P<0.05 compared with respective normoxia group by Student's *t* test (A,B) or one-way ANOVA (C,D).
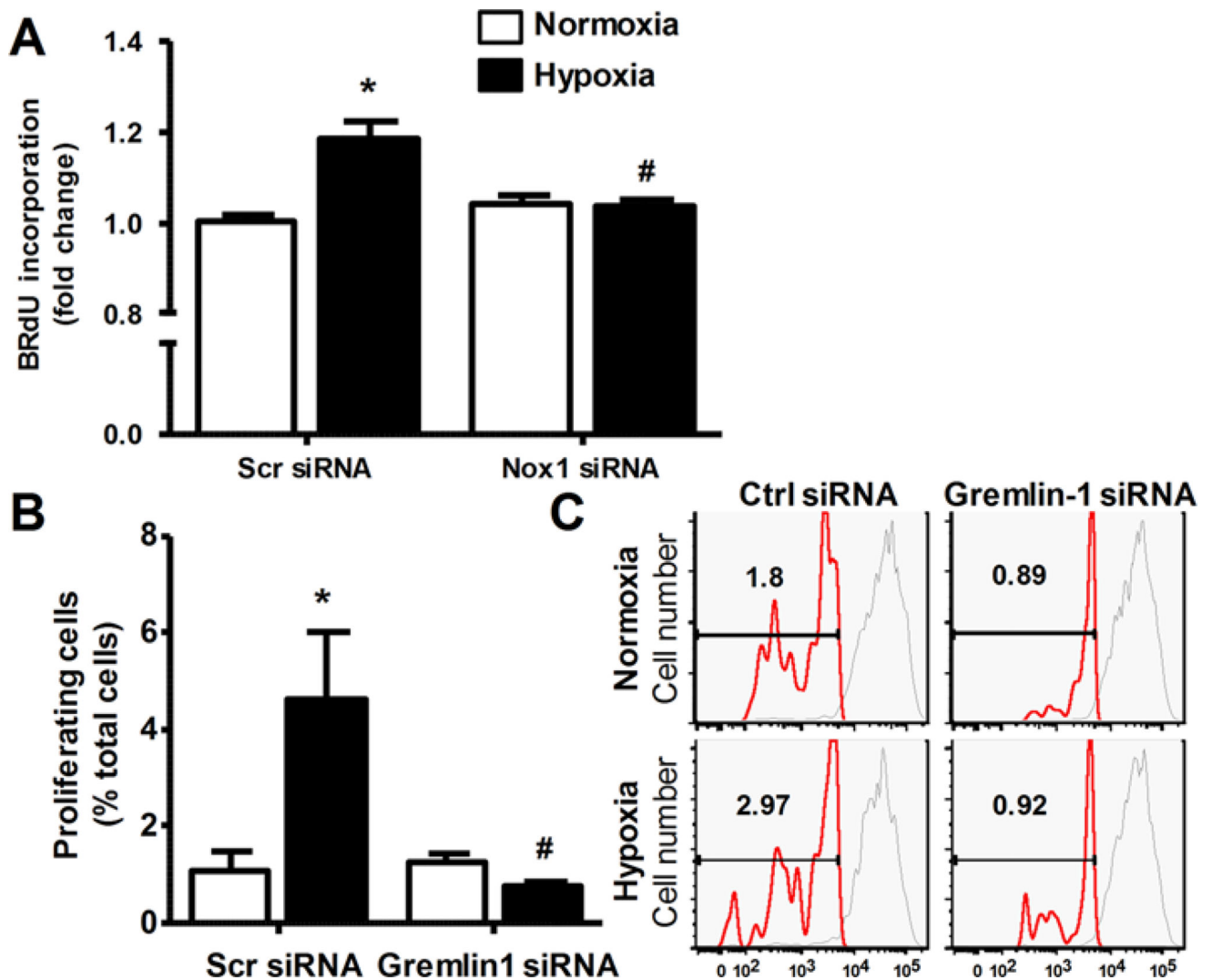
Figure 6. Loss of Nox1 or Grem1 attenuates hypoxia-induced HPAEC proliferation
HPAEC were transfected with Scr, Nox1 or Grem1 siRNA and exposed to hypoxia for 24 h.
(**A**) HPAEC proliferation was assessed by BrdU incorporation following transfection of cells
with Nox1 or Scr siRNA and subjecting them to 24 h hypoxia. Data are shown as means ±
S.E.M. of fold change relative to Scr normoxia control (n=6). (**B**) Proliferation of HPAEC
following transfection with Grem1 or Scr siRNA and 24 h hypoxia treatment was assessed
by the CFSE FACS assay. Data are shown as percent proliferating cells. (**C**) Representative
CFSE FACS tracings wherein the red spectrum indicates CFSE intensity in proliferating
cells and gray spectrum indicates non-proliferating controls (n=3). *P<0.05 compared with
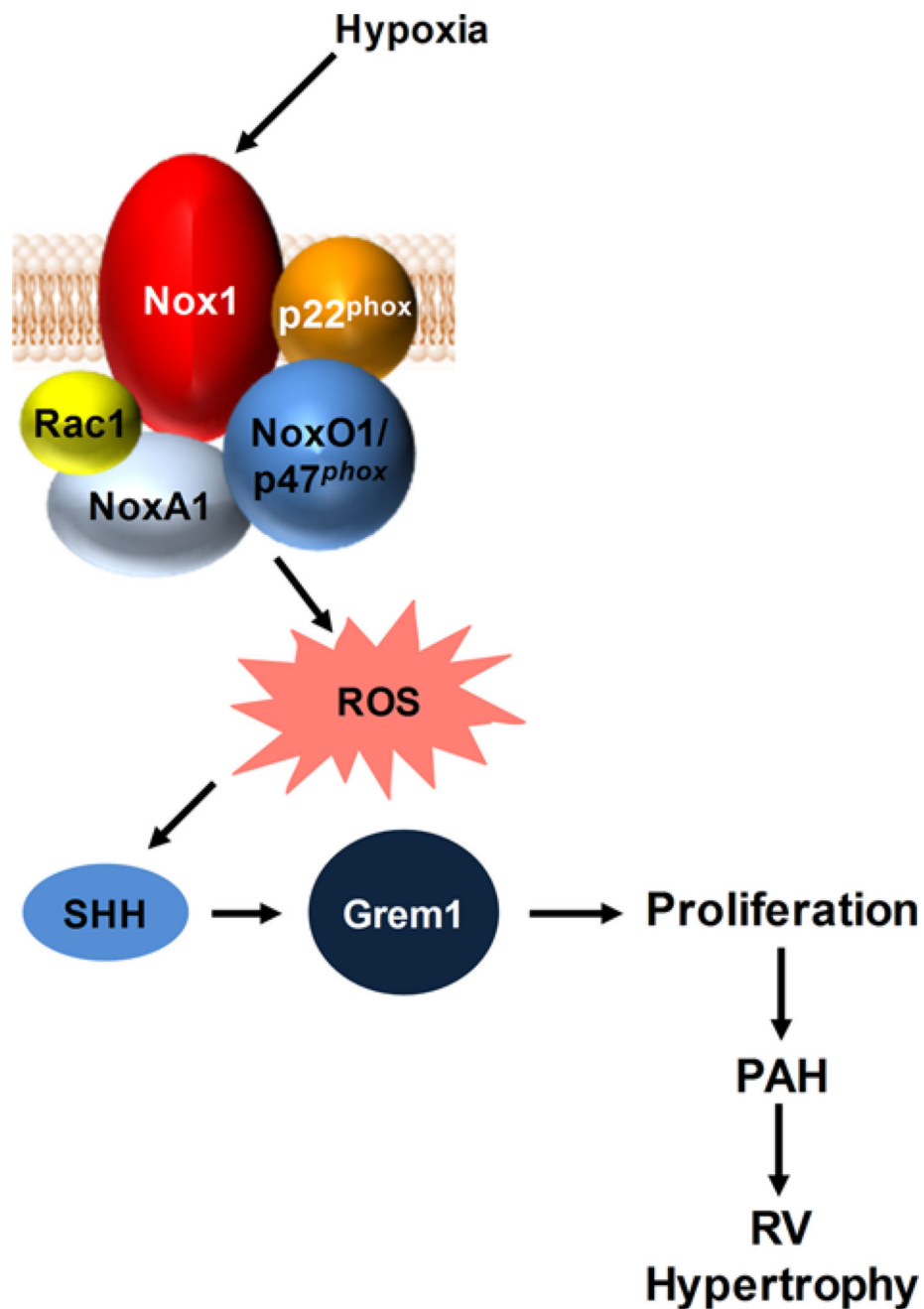Scr normoxia, #P<0.05 compared with Scr hypoxia.

Figure 7. Schematic diagram showing Nox1-Grem1 activation pathway in EC proliferation and RV hypertrophy

Hypoxia exposure of pulmonary ECs leads to Nox1-derived ROS production, which in turn activates SHH leading to Grem1 expression. This increase in Grem1 expression results in an unregulated proliferative process that ultimately leads to PAH and RV hypertrophy.

Table 1

Patient demographic and hemodynamic data

S.No.	Group	Age	Gender	Pathology	Hemodynamics	
					mPAP (mmHg)	TPG (mmHg)
	Non-PAH					
1		64	M			
2		62	M			
3		61	M			
4		65	M			
5		52	F			
6		42	F			
7		69	F			
	PAH					
8		64	M	IPF-PH	36	24
9		59	M	PAH	49	41
10		65	M	PAH	33	26
11		65	M	IPF-PH	29	28
12		51	F	Scleroderma-related PAH	53	40
13		66	F	Scleroderma-related PAH	44	34
14		43	F	Scleroderma-related PAH	31	23
15		65	F	PAH	55	43
16		37	F	PAH	85	73

TPG = mPAP − PCWP.

Values >12 are associated with PAH or with mixed-PH (pre- and postcapillary PH).

Abbreviations: IPF-PH, idiopathic pulmonary fibrosis-associated pulmonary hypertension; mPAP, mean pulmonary artery pressure; PCWP, pulmonary capillary wedge pressure; TPG, trans-pulmonary gradient.